Title: Detection of soil pipe network by geophysical approach:Electromagnetic induction (EMI) and electrical resistivitytomography (ERT)

Author: Anita Bernatek-Jakiel, Marta Kondracka

Citation style: Bernatek-Jakiel Anita, Kondracka Marta. (2022). Detection of soil pipe network by geophysical approach:Electromagnetic induction (EMI) and electrical resistivitytomography (ERT). "Land Degradation and Development" (2022), nr 79, s. 1-13, art. nr 4205. DOI: 10.1002/ldr.4205

RESEARCH ARTICLE

WILEY

Detection of soil pipe network by geophysical approach: Electromagnetic induction (EMI) and electrical resistivity tomography (ERT)

Anita Bernatek-Jakiel[1] | Marta Kondracka[2]

[1]Institute of Geography and Spatial Management, Faculty of Geography and Geology, Jagiellonian University, Kraków, Poland

[2]Institute of Earth Sciences, Faculty of Natural Sciences, University of Silesia, Katowice, Poland

Correspondence
Anita Bernatek-Jakiel, Institute of Geography and Spatial Management, Faculty of Geography and Geology, Jagiellonian University, Kraków, Poland.
Email: anita.bernatek@uj.edu.pl

Abstract

Studying soil pipes is a methodological challenge that needs improvement in detection methods in order to better recognize the role of piping erosion in land degradation and hillslope hydrology. This study explores electromagnetic induction (EMI) and electrical resistivity tomography (ERT) in order to identify soil pipes. The study was conducted in a mountainous area (the Bieszczady Mountains, SE Poland) under a temperate climate, where pipes develop in silty-clayey soils. In the plot area, eight profiles were measured by the conductivity meter at different depths and then interpolated to present apparent electrical conductivity (EC_a). Also, six ERT profiles were carried out using the Wenner-Schlumberger electrode configuration. The EC_a values measured by EMI are not very diversified, suggesting its lower sensitivity to changes in the EC_a, whereas the EC_a values measured by ERT are characterized by greater fluctuation, that is, better detection possibilities. ERT has revealed soil pipes as zones of higher electrical resistivity (ER >268 Ωm) than their surroundings (characterized below pipes by ER <105 Ωm) underlying the air filling of pipes (ER >427 Ωm), whereas EMI has revealed its higher sensitivity to water content. The EMI results have shown the lowering of the water table in the lower part of the slope, perhaps because of the drainage by a complex pipe network. EMI allows quick measurements of EC_a providing information on water content, and thus indirectly soil pipes, but, it cannot delineate individual pipes. Only the integration of geophysical methods supported by field recognition provides an effective method to detect soil pipes.

KEYWORDS
apparent conductivity, electrical tomography, electromagnetic induction, piping erosion, water content

1 | INTRODUCTION

Erosion by soil piping is an important land degradation threat around the world (Bernatek-Jakiel & Poesen, 2018; Poesen, 2018), although the subsurface nature of this process makes it difficult to study (Verachtert et al., 2011). There is a great need to develop methods for detecting soil pipes, including underground preferential flow paths because of their significance in soil erosion modeling, slope hydrology,

and civil engineering projects (Park & Jessop, 2018). Geophysical methods, which make exploration possible below the ground surface, are promising in soil piping studies. These methods are relatively cheap, time-efficient, and nondestructive to the ground surface (Schrott & Sass, 2008; Zajícová & Chuman, 2019). Their application in geomorphology normally requires the combination of different methods in order to avoid misunderstanding in data interpretation (Cardarelli et al., 2014; Schrott & Sass, 2008).

So far, various different geophysical methods have been explored in soil pipes detection, among which ground penetrating-radar (GPR) (Bernatek-Jakiel & Kondracka, 2016, 2019; Botschek et al., 2000; Got et al., 2014; Holden, 2004, 2006; Holden et al., 2002; Wodajo et al., 2021) and electrical resistivity tomography (ERT) (Ahmed & Carpenter, 2003; Bernatek-Jakiel & Kondracka, 2016; Bovi et al., 2020; Cardarelli et al., 2014; Giampaolo et al., 2016; Joshi et al., 2021; Leslie & Heinse, 2013; Patti et al., 2021) have received the most attention. These methods were tested to detect and visualize soil pipe networks, as well as to recognize the factors controlling piping erosion.

Electromagnetic induction (EMI) is widely used in soil studies to investigate soil properties that affect apparent electrical conductivity (EC_a) measured by EMI sensors (Doolittle & Brevik, 2014). The main soil properties possibly detected by EMI are water content, solution ions, and clays. Moreover, bulk density, soil structure, ionic composition, cation-exchange capacity (CEC), pH, soil organic carbon, nutrient, and $CaCO_3$ contents affect EC_a (McNeill, 1980). Despite its usefulness in detecting such different soil properties, EMI has been explored only to a limited extent in piping studies (Ahmed & Carpenter, 2003; Wodajo et al., 2021), although it has been proved that piping erosion is associated with several physical and chemical soil properties (Benito et al., 1993; Bernatek-Jakiel et al., 2016; Botschek et al., 2002; Faulkner, 2006; Verachtert et al., 2013). Moreover, and even more importantly, soil pipes as air-filled tunnels, sometimes with pipe flow, are sufficiently different from the surrounding soil to exhibit distinct electrical conductivity (Doolittle & Brevik, 2014).

Therefore, this study aims to detect soil pipe network by geophysical methods: EMI and ERT. The specific objectives are: (1) to recognize the geophysical response by ERT and EMI given by soil pipes and zones affected by piping erosion; (2) to compare EMI results with ERT profiles; and (3) to evaluate the suitability of EMI to detect the subsurface network of soil pipes, as this method was hardly ever used in such studies. The geophysical data have been correlated with field evidence of piping erosion and with high-resolution UAV-based digital elevation model (DEM). This study has been done in silty-clayey soils in a mountainous region under a temperate climate.

2 | STUDY AREA

The study was conducted in a small catchment called Cisowiec (388 ha) located in the Bieszczady Mtns. (SE Poland), the westernmost part of the Outer Eastern Carpathians (Figure 1a,b). The catchment is characterized by a mountainous landscape (elevation ranging
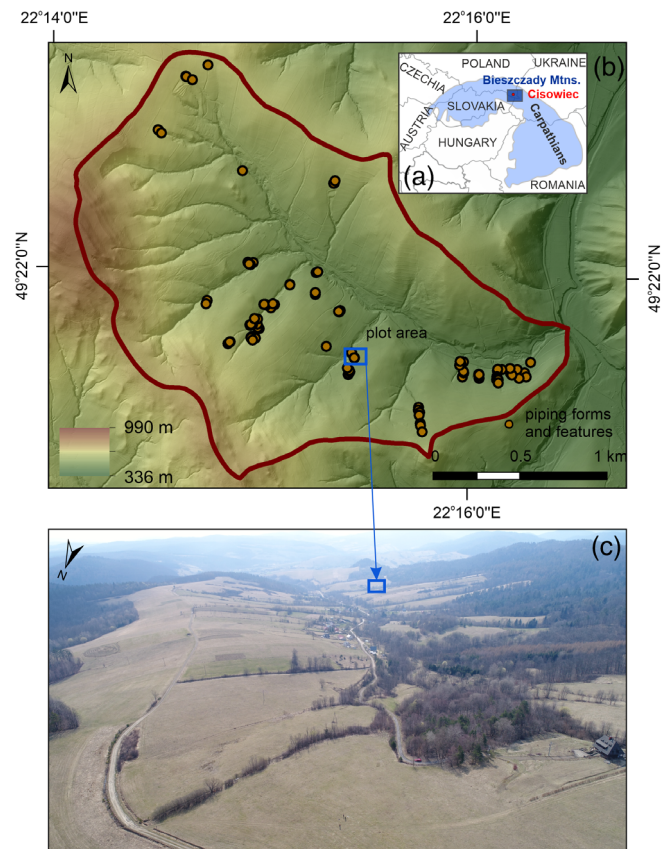

FIGURE 1 Location of the study area: (a) the regional overview, (b) the Cisowiec catchment with piping forms and features mapped and plot area marked, and (c) the oblique unmanned aerial vehicle (UAV) image of the Cisowiec catchment with plot area marked (photo: M. Liro) [Color figure can be viewed at wileyonlinelibrary.com]

from 400 to 742 m above sea level, average slope gradient is 15°). The slopes are mainly built of resistant flysch facies, that is, thick-bedded sandstones alternating with shales and mudstones, whereas the valleys are carved into less resistant flysch facies, that is, shales and mudstones (Haczewski et al., 2007). In the study area, soil pipes develop in Cambisols that develop from the slope deposits derived from flysch rocks with an eolian admixture (Kacprzak et al., 2015). The land use is dominated by forests (mixed forests with beech and occasionally with spruce) on steep slopes and by grasslands on gentle slopes (Figure 1c).

The climate is humid continental (according to the Köppen–Geiger climate classification) with a mean annual temperature of 7.0°C and a mean annual precipitation of 900 mm (according to data obtained from the Institute of Meteorology and Water Management-State Research Institute, IMGW-PIB, in Poland for the years 1960–2015 recorded at the Baligród–Mchawa and Terka weather stations).

The Cisowiec catchment has been already described as a piping-prone area, and details are provided by Bernatek-Jakiel and Kondracka (2019). In the catchment, 86 piping forms were mapped, including closed (sagging) depressions, sinkholes, and blind gullies (Figure 1b). The depth of soil pipe formation is 0.7–0.8 m at the soil–
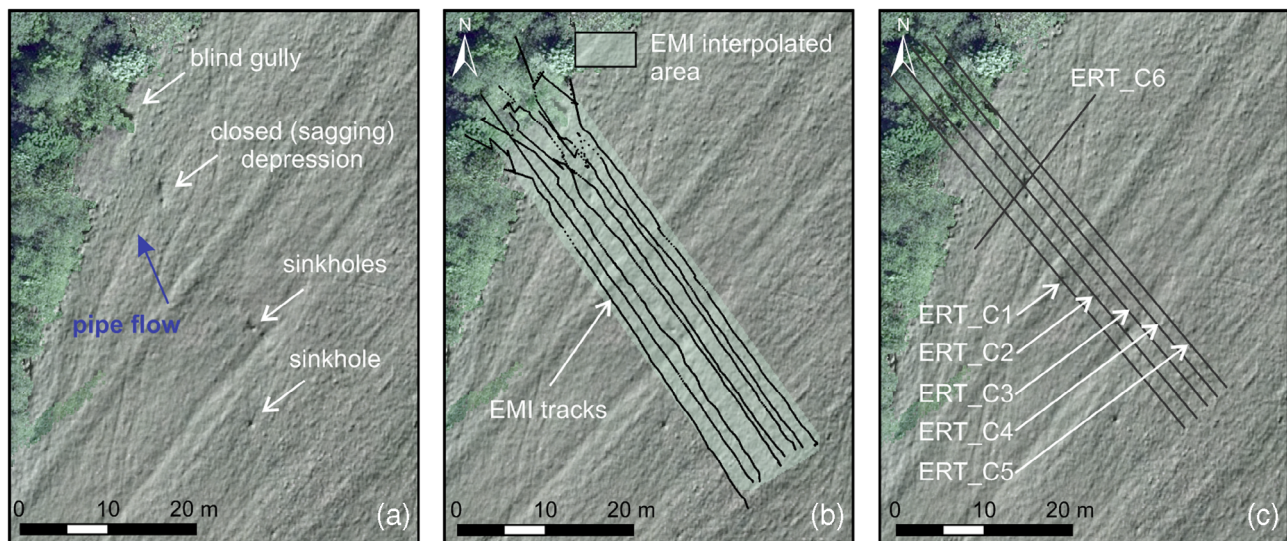
FIGURE 2 The plot area of detailed geophysical survey: (a) surface indicators of piping erosion, (b) the location of electromagnetic induction (EMI) tracks measured by the conductivity meter in the field and interpolated in ArcGIS, (c) the location of electrical resistivity (ERT) profiles measured by the Terrameter in the field (see the equipment in Figure 3) [Color figure can be viewed at wileyonlinelibrary.com]

FIGURE 3 A conductivity meter EM38-MK2 (a) and the LUND electrical imaging system with SAS 4000 Terrameter (b) used in the study area [Color figure can be viewed at wileyonlinelibrary.com]

bedrock interface. The size of the main pipe in the plot area is 0.2 × 0.3 m, and the smaller pipes are up to 0.02 m.

The detailed geophysical study (EMI and ERT) and UAV survey were conducted on the plot located in the SEE part of the catchment on a hillslope exposed to NW (Figures 1b,c and 2). The studied piping system is in grassland, and it ends at a pipe outlet in the forest. It consists of one closed (sagging) depression, three sinkholes, and one blind gully (Figure 2a). The length of this system is 44 m (measured from the most upslope pipe collapse, through the next, to the outlet). The pipes develop at a depth of 0.7–0.8 m.

3 | METHODS

To test the EMI and ERT in soil pipe network detection, we selected the plot area in the Cisowiec catchment (Figures 1 and 2), where

previously GPR survey had been done (Bernatek-Jakiel & Kondracka, 2019). The detailed EMI and ERT studies were carried out in November 2018, whereas the UAV survey was done in November 2019 (Figure 3). The integration of different geophysical methods gives a great opportunity for cross-checking acquired data and reducing interpretation ambiguities (Cardarelli et al., 2014; Schrott & Sass, 2008). In order to compare subsurface data obtained from geophysical methods with the surface response (i.e., depressions and collapses), the field mapping of piping forms was done (Bernatek-Jakiel & Kondracka, 2019), and high-resolution DEM and orthophotos have been produced. The UAV flights were carried out using a DJI Phantom-4 quadcopter with a 1′ camera. The images were taken from a low altitude, and they were processed using the structure from motion (SfM) technique (AgiSoft software). The UAV-derived products (orthophotos and DEM) have a resolution of 0.014 × 0.014 m.

Vertical mode

Coil separation: 1 m and 0.5 m
V-mode depth exploration: 1.5 m and 0.75 m

Horizontal mode

Coil separation: 1 m and 0.5 m
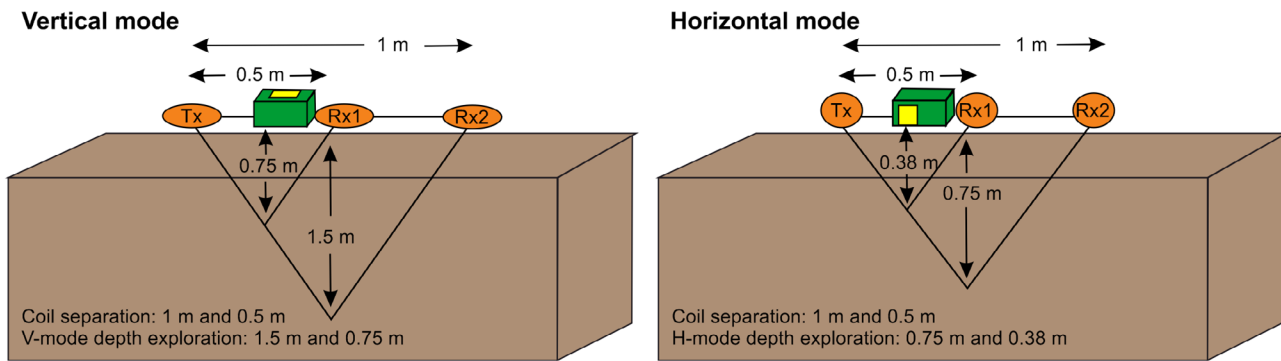H-mode depth exploration: 0.75 m and 0.38 m

FIGURE 4 A conductivity meter EM38-MK2 coil schematic in vertical (V-mode) and horizontal (H-mode) mode, where Tx, Rx—Transmitter and receiver coil, respectively. Operating frequency: 14.5 kHz [Color figure can be viewed at wileyonlinelibrary.com]

TABLE 1 The EM38-MK2 effective depth range of conductivity measurements with different coil orientations

Coil orientation	0.5 m coil separation	1 m coil separation
Vertical dipole	0.75 m	1.5 m
Horizontal dipole	0.37 m	0.75

Source: Producer's website: https://www.geomatrix.co.uk/land-products/electromagnetic/geonics-em38mk2/ (access date: 04.01.2022, modified)

3.1 | Electromagnetic induction

Several advantages of EMI such as its speed, ease of use, relatively low cost, and volume of data collected make this method useful in soil studies. Generally, EMI sensors measure changes in EC_a of the subsurface (Doolittle & Brevik, 2014). In this study, the measurements were carried out using a conductivity meter EM38-MK2 (Geonics) in both vertical and horizontal measuring dipole orientations (Figures 3a and 4). The EM38-MK2 provided simultaneous measurements of EC_a with two transmitter receiver coil separation (0.5 and 1 m) that enables a penetration depth of up to 1.5 m with measurements at 0.75 m in both coil orientations (Table 1). These depths correspond to the depth of soil pipe occurrence in the study area, that is, the average depth of soil pipe development is 0.7–0.8 m with maximum of up to 1.5 m.

In the plot area, eight profiles were measured by the conductivity meter along the slope, approximately longitudinally to the piping system (Figure 2b). The conductivity meter was carried by a measurer at a height of 0.4 m above the ground. The collected data were processed using the DAT38MK2 software (Geonics Ltd.). The software also made it possible to gather profiles and create a GPS-based XYZ file for further interpretation. Then, the data were interpolated in ArcGIS version 10.8 using the nearest neighbour interpolation approach. The interpolated data were presented on maps using different symbology: natural breaks (Jenks) in order to underline all the differences in EC_a, and stretched symbology with the same minimum and maximum values in order to facilitate the comparison of results. EMI conductivity maps were plotted for both vertical dipole (V-mode)
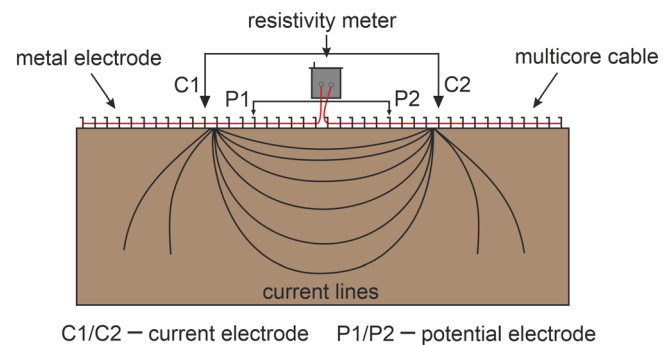

FIGURE 5 A schematic diagram of the electrical resistivity tomography (ERT) equipment used in the study [Color figure can be viewed at wileyonlinelibrary.com]

and horizontal dipole (H-mode) coil orientations to differentiate near-surface from deeper response.

3.2 | Electrical resistivity tomography

ERT provides high-resolution images of the subsurface revealing the variation in electrical resistivity (ER, inverse of electrical conductivity). The electrodes are normally placed on the ground surface (Figures 3b and 5). The current is injected into the ground through two current electrodes (C1 and C2), and the resulting voltage difference at two potential electrodes (P1 and P2) is measured. The apparent resistivity (ρ_a) value is calculated from the current (I) and voltage (V) values (Figure 5).

$$\rho_a = k \, V/I.$$

Where: k is the geometric factor, which depends on the arrangement of the four electrodes (C1, C2, P1, P2; Loke, 2000).

In this study, ERT profiles were performed using the LUND electrical imaging system with the SAS 4000 Terrameter produced by ABEM Malå (Guideline Geo). Data acquisition was replicated with an

electrode spacing of 0.8 m using the Wenner-Schlumberger electrode configuration, which is moderately sensitive to both horizontal and vertical structures, and has better horizontal coverage and signal strength than other arrays (Loke, 2004). During the fieldwork, five ERT (ERT_C1–C5) profiles oriented approximately parallel to the piping system, and one transverse profile (ERT_C6) was carried out (Figure 2c).

The measured apparent resistivity data were interpreted with the Res2DInv software (Geotomo Software). The software uses an iterative smoothness-constrained least-squares method to create a model of resistivity of the subsurface. The resulting models were based on 126 points for profile ERT_C6, 412–555 points for profiles ERT_C2 and ERT_C3, and 646–660 points for profiles ERT_C1, C4, C5. The root-mean-squared error (RMS), which indicates the differences between the calculated and measured values of apparent resistivity in the model, varied from 0.4% to 6.8% for the 5th iteration. RMS error was higher for profiles, where more pipes were observed.

3.3 | EMI and ERT comparison

In order to compare quantitatively EMI and ERT methods, EC_a measured by the conductivity meter EM38-MK2 and the SAS 4000 Terrameter has been compiled as a graph. The EC_a values from the ERT profiles were taken from the following depths: 0.45, 0.77, and 1.49 m, which correspond to the depth of EMI measurements, that is, 0.37, 0.75, and 1.5 m. The EMI traces aligned the closest to the ERT profiles were used for the comparison. This allowed comparing the electrical patterns of ERT and EMI results.

4 | RESULTS

The geophysical results are presented in relation to the high-resolution topography derived from the UAV survey. The UAV-based DEM was used to prepare a hill-shade as a base map for EMI conductivity maps, and ERT profiles were verified with surface topography.

4.1 | EMI results

EMI conductivity maps plotted for both V-mode and H-mode using different symbology are presented in Figures 6 and 7. Generally, the conductivity of the subsurface increases with depth (Figure 6), from 10 mS m^{-1} (in H-mode) near the surface (at a depth of 0.37 m) up to >100 mS m^{-1} (in V-mode) at a depth of 1.5 m. The lowest EC_a values are noted at a depth of 0.37 m (Figures 6 and 7). The analysis of the near surface in H-mode reveals the zones of lower EC_a (<15 mS m^{-1}) in the upper part of the slope and around sinkholes. Higher EC_a values (15–20 mS m^{-1}) are seen around the closed (sagging) depression in the lower part of the slope and the highest EC_a values (up to >100 mS m^{-1}) in the blind gully near the forest edge. A similar trend is observed at the depth of 0.75 m (Figure 7). The lower EC_a values in the forest are related to the sandstone outcrops in this area.

In V-mode, in which sensitivity to variations increases with depth, it can be observed that EC_a values increase around the sinkholes, the closed (sagging) depression, and the blind gully with depth. The zone of higher EC_a values covers a bigger area at greater depth (especially in the upper part of the slope), that is, 1.5 m, and is associated with pipe network (Figure 7).

4.2 | ERT results

ERT profiles ERT_C1–C5 (longitudinal, oriented approximately parallel to the piping system, 56.8 m long) reach a maximum depth of about 6.30 m in the central zone (Figure 8). The near surface layers are characterized by higher ER (>427 Ωm), whereas the lower layers are highly conductive materials (ER <105 Ωm) with zones of low ER (<26 Ωm). These zones of low ER values indicate probably shales or mudstones and are characterized by higher water content than the surroundings. There is a zone of high ER values in ERT_C2 (depth of 4–6.3 m in the forest near the grassland boundary), which is on the surface in ERT_C1. This anomaly is related to the sandstone outcrops. Also, the upper part of the slope (at the distance above 45 m from the beginning of ERT profiles) is characterized by higher ER values (Figure 8).
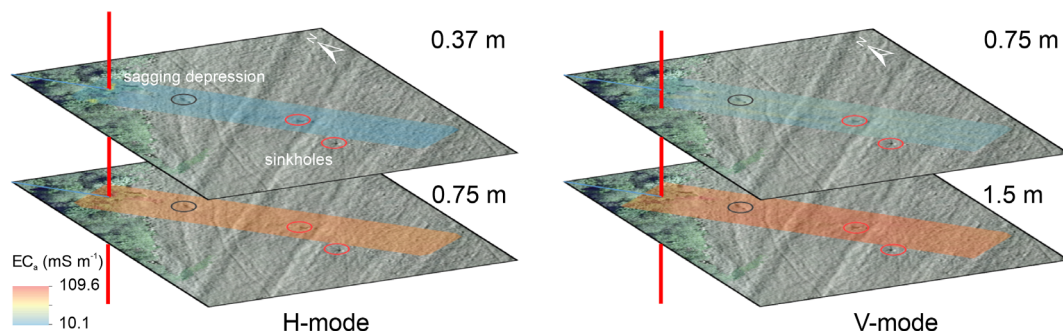

FIGURE 6 Electrical conductivity measured by the conductivity meter in the study area in horizontal mode (H-mode, at two depths: 0.37 and 0.75 m) and in vertical mode (V-mode, at two depths: 0.75 and 1.5 m) presented as pseudo 3 model using stretched symbology with the same minimum and maximum values [Color figure can be viewed at wileyonlinelibrary.com]
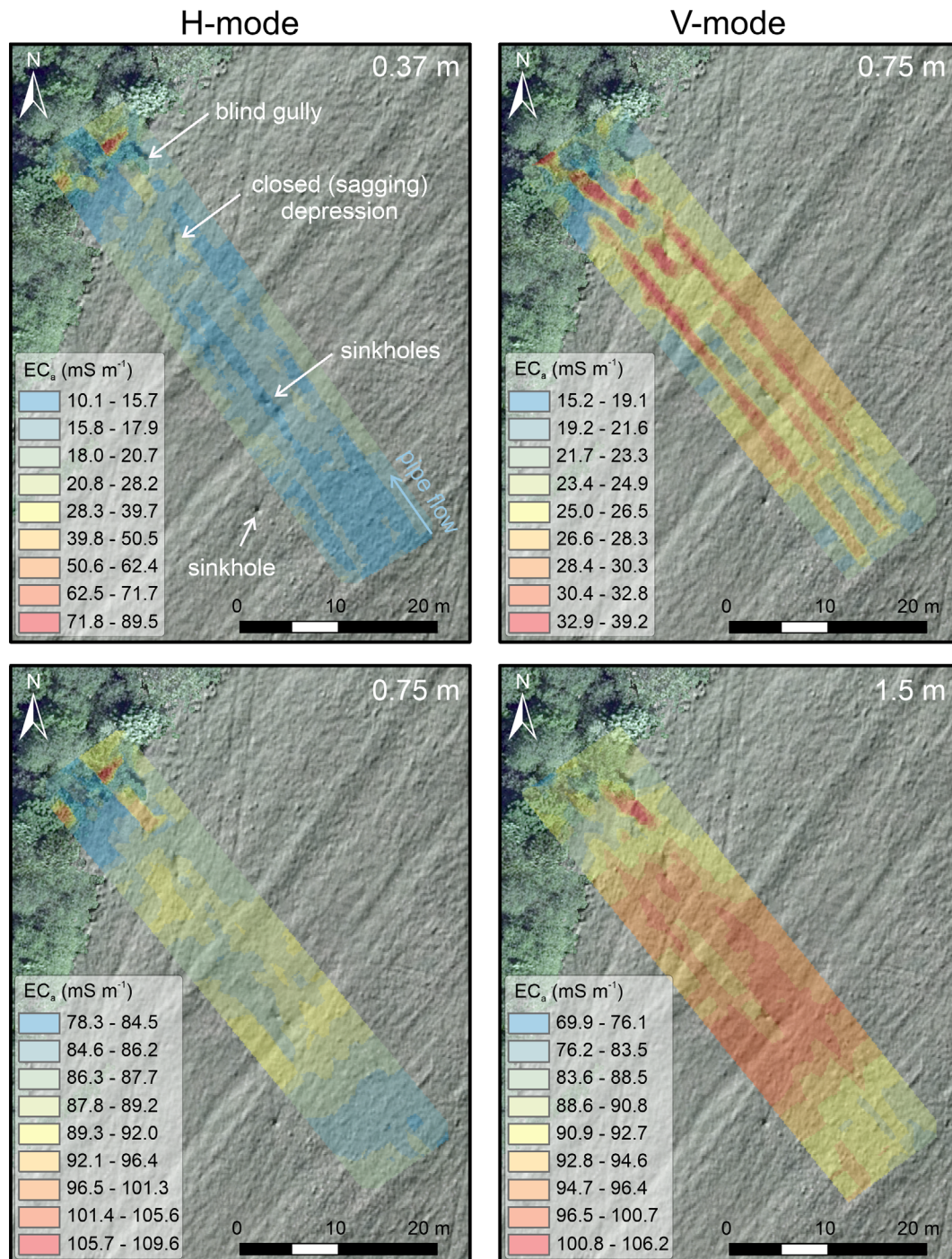
FIGURE 7 Electrical conductivity measured by the conductivity meter in the study area in horizontal mode (H-mode, at two depths: 0.37 and 0.75 m) and in vertical mode (V-mode, at two depths: 0.75 and 1.5 m) classified using natural breaks in order to underline all the differences in electrical conductivity [Color figure can be viewed at wileyonlinelibrary.com]

Pipes in ERT profiles are marked by higher ER values, as is especially well seen in ERT_C2 and ERT_C3, which undoubtedly intersected soil pipes in the field (Figure 2c). In ERT_C2 and ERT_C3, there is an anomaly of high ER (>427 Ωm, marked by a yellow line in Figure 8), which is probably associated with ground disturbed by piping erosion (up to 1 m deep). This anomaly is also slightly marked in ERT_C3, which was done just near the surface piping forms and

features. Profile ERT_C4 crossed the blind gully bottom (Figure 9)—from 7.2 to 10.8 m (Figure 8). There are small zones of higher ER values just below and just above this form (in the gully wall) indicating the pipe occurrence. In ERT_C5, there is also a zone of higher ER below a blind gully (in the forest) indicating soil pipes.

Profile ERT_C6 (19.2 m long and 3.5 m deep) was carried out transversely to the piping system, and it intersected a sagging
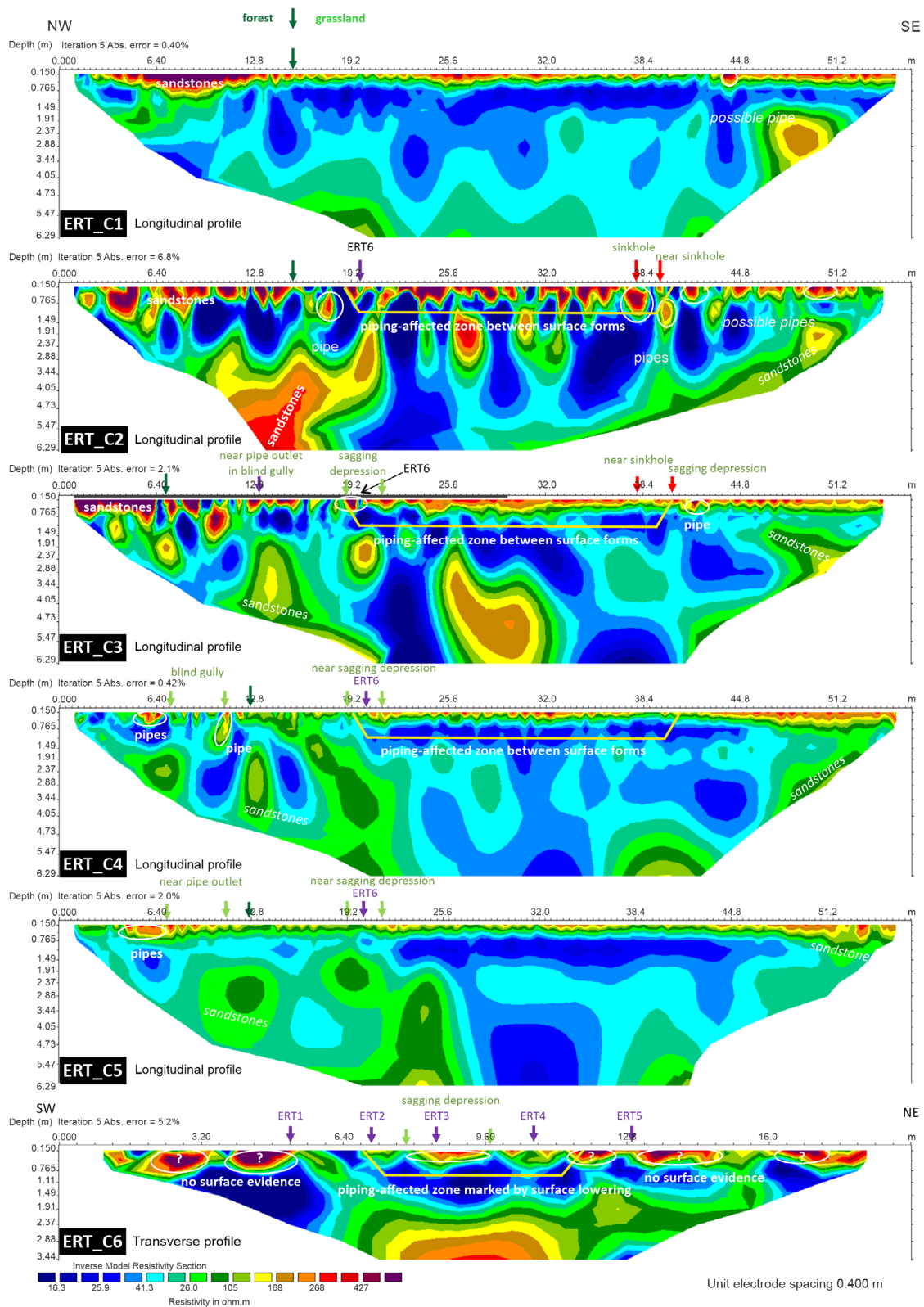
FIGURE 8 Electrical resistivity tomography (ERT) profiles made in the study area. ERT_C1–C5 are longitudinal profiles, whereas ERT_C6 is a transverse profile to the piping system. The location of piping forms and features visible on the surface is marked in green. The boundary between forest and grassland is marked by dark-green arrow [Color figure can be viewed at wileyonlinelibrary.com]
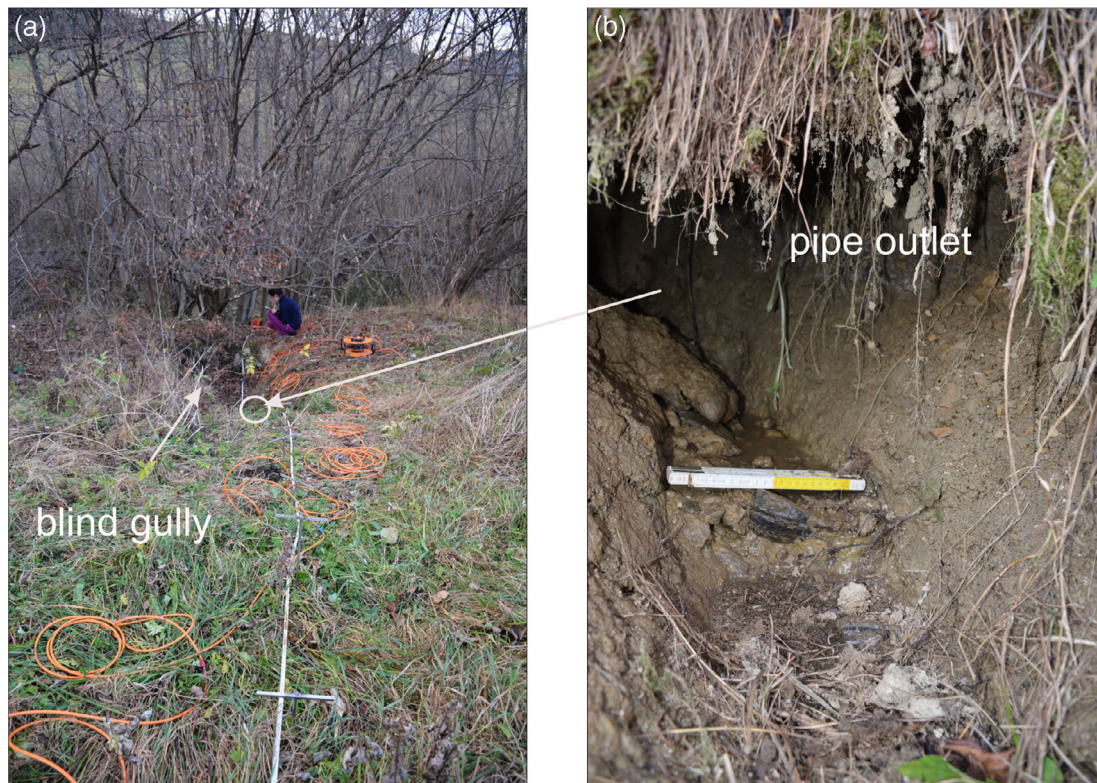
FIGURE 9 Blind gully near the forest edge (a) with the pipe outlet (b) and water flows in the bottom of a pipe (photo: A. Bernatek-Jakiel) [Color figure can be viewed at wileyonlinelibrary.com]

depression (Figure 2c). This sagging depression is underlaid by one zone of higher ER (>168 Ωm). However, the surrounding surface is slightly lowered (marked by a yellow line in ERT_C6 in Figure 8), and it corresponds to the subsurface response, that is, several small zones of higher ER values. It may indicate the existence of several pipes that accompany the main one which caused the clear sagging depression. There are more zones of higher ER values, but they are not expressed by the surface depressions or collapses (Figure 8).

4.3 | Comparison of EMI and ERT results

The EC_a values measured by the EMI and ERT devices are compiled (Figure 10). The most interesting thing here is the electrical pattern, that is, the distribution of EC_a values along the profile with the peaks on the graphs that indicate the anomalies associated with soil pipe occurrence (water content and air filling). Generally, the EC_a values measured by the EMI device are not very diversified (the span of EC_a values is from 6 to 33 mS m^{-1} with a maximum of up to >110 mS m^{-1} measured in the blind gully, Figures 9 and 10), whereas the EC_a values measured by the ERT device are characterized by greater fluctuation (from 22 to 132 mS m^{-1}) and several peaks (up to >330 mS m^{-1}, Figure 10). This suggests a higher sensitivity of ERT than EMI in the given conditions, which results in better detection of soil pipes by ERT. The peaks of EC_a measured by ERT achieved the highest values (>320 mS m^{-1} on profile ERT_C2, >120 mS m^{-1} on

profile ERT_C3, and > 60 mS m^{-1} on profile ERT_C4) in places where water is at the bottom of a pipe, as water is characterized by high EC_a. This is for instance clearly visible on profile 2, where a highest peak indicates the pipe flow at the beginning of piping affected zone, on profile 3 where peaks refer to the pipe outlet and the beginning and end of a sagging depression, as well as on profile 4 in a blind gully (Figure 10). The peaks of EC_a measured by ERT, which are clearly visible on the graphs (Figure 10), mean that the pipe flow has been detected by this device. The interpretation of zones with low EC_a (i.e., high ER) is difficult to observe on the graphs (Figure 10) owing to the high variability of values in comparison with the ERT profiles (Figure 8), where such zones as indicators of air-filled pipes are clearly visible.

5 | DISCUSSION

5.1 | Geophysical response of soil pipes and their surroundings

The general geophysical response of the subsurface in the study area is similar both on the ERT profiles and EMI maps (Figures 6, 7 and 8). In the ERT profiles, the near surface is characterized by higher ER that decreases with depth (up to 1.5 m, Figure 8). Similarly, the EC_a of subsurface presented on the EMI maps increases with depth (Figure 6a). This is related to biological activity (vegetation and animal burrows) in
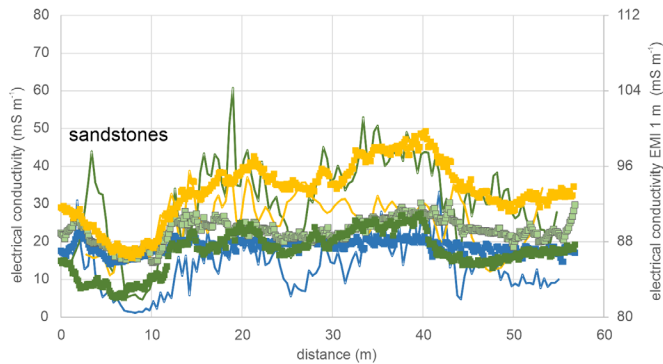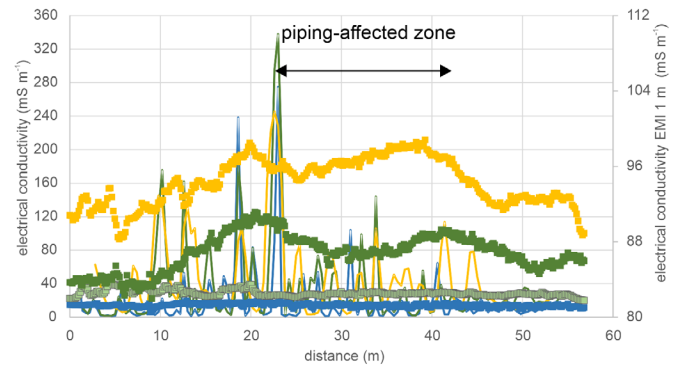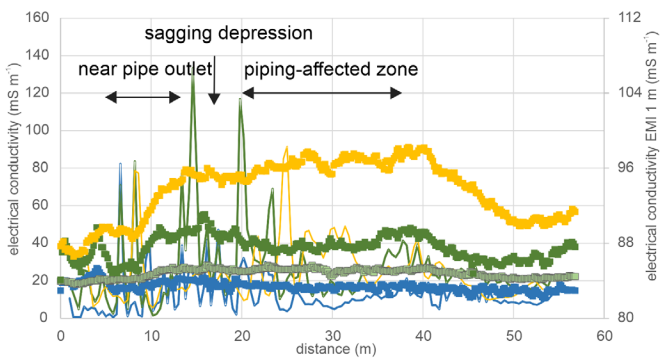
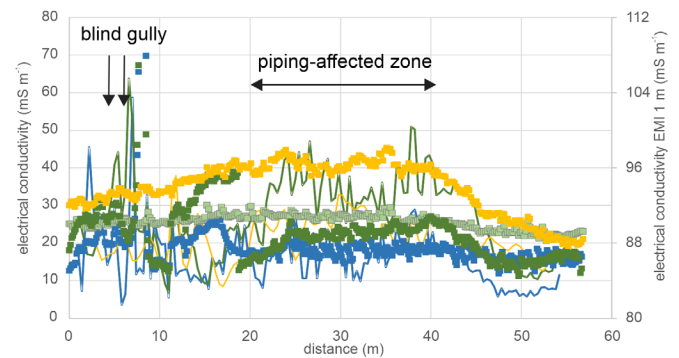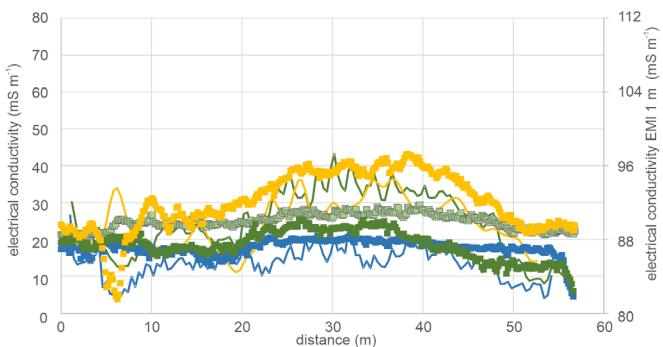**FIGURE 10** The comparison of apparent electrical conductivity (EC$_a$) measured by the electromagnetic induction (EMI) and electrical resistivity tomography (ERT) devices [Color figure can be viewed at wileyonlinelibrary.com]

the near surface, thus the occurrence of roots and air-filled macropores. The lower values of ER and higher values of EC$_a$ in deeper layers may be connected to higher water and clays content that increases down the undisturbed soil profile (not affected by piping). These trends in soil profiles have been recently presented by Bernatek-Jakiel et al. (2020) in the vicinity of the plot analyzed in this study. This is connected with the water table which occurs at the depth of 1–1.1 m.

In line with previous studies (Ahmed & Carpenter, 2003; Bernatek-Jakiel & Kondracka, 2016; Bovi et al., 2020; Cardarelli et al., 2014; Giampaolo et al., 2016; Joshi et al., 2021; Leslie & Heinse, 2013; Patti et al., 2021), soil pipes in the study area are presented as zones of higher ER on the ERT profiles (Figure 8) because the air filling the pipes behaves as an insulator (Samouëlian et al., 2005). In the study area, ER above 268 Ωm indicates the zones affected by piping

erosion, whereas clear pipes are marked by ER >427 Ωm (Figure 8). For instance, Bovi et al. (2020) in tropical humid forests in Brazil found zones with ER > 4000 Ωm to be soil pipes, and Joshi et al. (2021) in the humid Western Ghats in India interpreted zones with ER > 1800 Ωm as soil pipes. On the one hand, this suggests that the general geophysical response of soil pipes is the same, that is, with higher ER values than the surroundings. On the other hand, there are no strict values of ER that indicate air-filled pipes, but it is rather the relative values, which depend on soil and bedrock properties in a given region as well as the water condition in the subsurface during a field survey. In the study area, it is characteristic that just below the identified pipes and larger areas affected by piping erosion (Figure 8), there are zones with the lowest resistivity values. This may be because of the concurrent effect of shale/mudstone layers that create a water restrictive layer and the content of water that flows at the

pipe bottom. Both conditions result in lower ER values (Bernatek-Jakiel & Kondracka, 2016). In other areas, low resistivity zones directly below the sinkholes were related to the weathered bedrock fractures (Ahmed & Carpenter, 2003) or to wetter zones, sometimes water-filled pipes (Bovi et al., 2020). It is worth nothing that sometimes, when soil pipes occur within already high restrictive layers, their geophysical response is not clear enough to delineate them by the ERT (Leslie & Heinse, 2013). It means that ERT, although in many places around the world it provides satisfactory results on pipe detection, is not a universal method.

Interestingly, on the EMI maps zones, affected by piping erosion in the lower part of the slope, are marked as areas of higher EC_a, that is, lower ER than their surroundings (Figure 7). It suggests that the EMI sensor catches mainly higher water content around the pipes and the water that flows in the bottom rather than the air filling the pipes (Figure 9). Moreover, this also implies that probably the pipes filled by air in the study area are too small to be caught by the EMI sensor. This is in line with the study by Ahmed and Carpenter (2003), who noted enhanced soil moisture in the vicinity of active soil pipes, which resulted in high EC_a values recorded over these features. However, it is in contrast with the latest study of Wodajo et al. (2021), who observed all the surface features (gully windows and depressions) of soil piping within low EC_a values. In the study area, only around the sinkholes in the upper part of the slope are there zones of lower EC_a (Figure 7). This may be related to the absence of water in the bottom of a pipe in that position during the fieldwork and with the higher porosity associated with piping affected soils. It is worth noting that a large area of the upper part of the slope is characterized by higher water content at 1.5 m depth ($EC_a > 90$ mS m^{-1}) than the lower part of the slope ($EC_a < 70$ mS s^{-1}). It suggests the position of the water table, which is lowered in the lower part of the slope, perhaps because of the drainage by several pipes. According to the previous studies, soil pipe networks become more complicated and complex down the slope (Bernatek-Jakiel & Kondracka, 2019), so they concentrate the subsurface flow and drain the area. Anyway, it also implies that the interpretation of EMI results is not straightforward, and as stated recently by Wodajo et al. (2021), the EMI sensor lacked the resolution to delineate individual soil pipes.

It has to be added that the EC_a values measured by ERT and EMI (Figure 10) differ, that is, EMI gives values between 0 and 110 mS m^{-1}, whereas ERT up to >360 mS m^{-1}. This indicates not only different sensitivity but also the intrinsic instrumental resolution limit of the devices. The conductivity values measured by the EMI and then processed are not directly comparable with the ERT resistivities (changed into EC_a values) in terms of absolute values but rather in terms of electrical pattern. Generally, the electromagnetic methods are more complicated, and the data are more sensitive to distortions, for example, electronic instrumental drift, unintentional heterogeneous height and orientation of the device during field survey, variations of ground surface cover (e.g., vegetation height), and an abundance of macropores in the near surface. This is in line with recent studies of rock glaciers in the Dolomites (Pavoni et al., 2021), where ERT and EMI methods were compared.

Our research aims to improve the detection of soil pipes using different geophysical methods. At the study site, we have already tested GPR to identify soil pipes and to present the complexity of soil pipe networks (site C in Bernatek-Jakiel & Kondracka, 2019). The ERT profiles correlate well with the GPR profiles, that is, soil pipes visible on the GPR profiles as hyperbolas are seen on the ERT profiles as zones of higher ER. Moreover, GPR verifies the zones of high ER values visible on the ERT profiles, which are interpreted as sandstones (nonpipes), for example, on profile ERT_C1 (= GPR_C5 in Bernatek-Jakiel & Kondracka, 2019), there is a zone with high ER values that are not seen as hyperbolas on GPR_C5. This proves that the combination of different geophysical methods gives a better interpretation of the subsurface (Schrott & Sass, 2008).

5.2 | Suitability and limitations of EMI for the exploration of soil pipes

This study has explored the use of EMI in soil pipes detection in comparison to ERT. Soil pipes are more clearly visible on the ERT profiles (Figure 8) than on the EMI maps (Figure 7), which is also confirmed by the graphs that compiled EC_a values measured by the EMI and ERT devices (Figure 10). As already mentioned, soil pipes are detected as zones of higher ER on the ERT profiles (Figure 8), whereas on the EMI maps in the lower part of the slope they are marked as areas of higher EC_a (lower ER) and in the upper part of the slope as areas of lower EC_a than their surroundings (Figure 7). It suggests that EMI cannot unambiguously detect a soil pipe network in the study area. The different response of soil pipes on the EMI maps complicates the interpretation of data and requires surface indicators of piping erosion that may clear up the doubts. Moreover, the EC_a reading presenting on the EMI maps is a weighted average value across a depth range (in our case: 0.37, 0.75 and 1.5 m), whereas ERT provides absolute values for local conductivities as a function of depth (Foley et al., 2012; Lavoué et al., 2010). Pipes that are filled both by water and air resulted in a sharp boundary of electrical conductivity (two media of opposing conductivity), but perhaps the size of this difference was too small to be clearly caught by the EMI sensor used, whereas for the ERT, it was sufficient. In this study, the EMI device is more sensitive to water content than to the air that fills the pipes. Also, the published reports on the EMI application in soil piping studies suggest that the EMI gives a different geophysical response of soil pipes (Ahmed & Carpenter, 2003; Wodajo et al., 2021). The question remains open as to whether the different coil separation and the height of the EMI device will improve the obtained results. It requires further studies.

The high sensitivity to water content of the EMI device has been already underlined. Marey and Tola (2015) showed the significant differences in the measured EC_a under different soil moistures for both coil orientations in relation to the height of the EM38 device above the ground. They observed that the highest measurement accuracy was obtained at the highest tested soil moisture (i.e., 24.5%). In the study area, the soil moisture is generally above 30% (Bernatek-Jakiel et al., 2020), which may suggest sufficient measurement accuracy.

In the EMI survey, there is a large difference in the response to near surface material in the two coil configurations, that is, the H-mode is relatively sensitive to variations in the near surface, whereas the V-mode is insensitive. Generally, in the V-mode, the relative sensitivity increases with depth, becomes a maximum at about 0.4 m (0.2 m for 0.5 m coil separation), and decreases slowly thereafter, whereas in the H-mode, it is greatest at the surface and decreases with depth (Heil & Schmidhalter, 2015). This means that in the H-mode, a map of 0.37 m is more reliable than a map of 0.75 m, even though the obtained results have revealed the same trend at both depths, that is, pipes in the lower part of the slope are associated with higher EC_a in contrast to the pipes in the upper part of the slope. It is similar in the V-mode (Figure 7). Anyway, the EMI device allows the quick measurement of EC_a at different depths and different coil configurations, so this limitation is reduced, and even more, it resulted in more accurate information at different depths.

As presented above (Figures 3a and 4), a conductivity meter is carried by a measurer at a given orientation (vertical or horizontal) and height of the dipole, which is set at the beginning of the measurements. However, it may result in unintentional human errors as some variations of orientation and height of the EMI device may occur and add noise to the measurements (Rejiba et al., 2018). This problem does not occur during ERT measurements as the electrodes are set up in the ground, and they are not moved during the survey. This also implies that the data of ERT and EMI cannot be directly compared, as has been already mentioned and reported by Pavoni et al. (2021).

Recently, Kim et al. (2020) tested a small-loop electromagnetic survey to check the position and depth of the cavities on the ER models. Such objects were detected as zones of higher ER, but interestingly their actual position was a little bit lower than these zones of lower ER. This theoretical study suggests that also in this research, the actual position of soil pipes may be deeper than detected by ERT and probably EMI.

In the study area with silty-clayey soils characterized by high soil moisture (as in this case), EMI can be an accompanying and supporting method that provides information on water content, thus indirectly indicating the occurrence of soil pipes and the susceptibility to piping erosion. It cannot delineate individual soil pipes. These findings correspond with the latest study by Wodajo et al. (2021), who stated that EMI provides zoning information on soil piping susceptibility, but it only narrows down the locations for more focused and intrusive investigation. It is in line with studies done in different geomorphological contexts, for example, rock glaciers, where also EMI has been suggested for use as an instructive method to extend, in a quick and convenient way, the information derived from the more accurate ERT technique (Pavoni et al., 2021). This study has proved that the use of at least two geophysical methods (here EMI and ERT) may give a sufficient insight to avoid misinterpretation as already underlined in geomorphological studies (Schrott & Sass, 2008). The interpretation of geophysical data is often ambiguous and requires good field recognition.

6 | CONCLUSIONS

The detection of a soil pipe network is a methodological challenge not only in soil erosion studies but also in hydrological, geomorphological, and civil engineering ones. This study tested the EMI method in comparison to ERT in the silty-clayey mountainous area under a temperate climate. The integration of EMI and ERT data supported by the field recognition of piping forms, and the UAV-based DEM provides an effective method to detect soil pipe network in the study area and gives interesting results on hillslope hydrology.

Soil pipes as tunnels filled by air and with water flow at the bottom (in the lower part of the slope during the survey) are detected by geophysical methods. These significant differences between pipes and their surroundings (in terms of the passage of electromagnetic waves) have been easily detected by the ERT. The ERT has revealed soil pipes and larger areas affected by piping erosion as zones of higher ER than surroundings (ER >268 Ωm). However, the interpretation of such zones has to be supported by field data as a similar geophysical response is given by sandstone outcrops. Moreover, soil pipes may be characterized by different ER values depending on soil and bedrock properties and moisture conditions in the given study area. The general electrical pattern is that soil pipes on the ERT profiles are characterized by higher ER than their surroundings. However, the interpretation of absolute values should be always compared to the local conditions, and it cannot be directly compared to other regions.

In the case of EMI, the detection of soil pipes is more complicated, and the data interpretation is not straightforward. The EMI device (EM38-MK2) tested in this study has revealed its higher sensitivity to water content than to air filling the pipes. In the lower part of the slope, soil pipes are marked as areas of higher EC_a, whereas in the upper part of the slope as areas of lower EC_a. This is associated with the water content, that is, the absence of pipe flow in the upper part of the slope during the geophysical survey. Moreover, the EMI results have shown the lowering of the water table in the lower part of the slope, probably because of the drainage by a complex soil pipe network.

This investigation illustrates the suitability and limitations of EMI. The EMI method allows quick measurements of EC_a at different depths providing valuable information on water content, thus indirectly indicating the occurrence of soil pipes and the susceptibility to piping erosion. It cannot delineate individual soil pipes. It has to be always integrated with other geophysical methods and good field recognition.

under the program "Excellence Initiative—Research University" at the Jagiellonian University in Kraków.

We thank Maciej Liro (The Institute of Nature Conservation of the Polish Academy of Science) for preparing the high-resolution DEM and ortophotos using the UAV.

DATA AVAILABILITY STATEMENT

The data that support the findings of this study are available from the corresponding author upon reasonable request.

ORCID

Anita Bernatek-Jakiel https://orcid.org/0000-0001-9691-2159
Marta Kondracka https://orcid.org/0000-0001-8897-5678

REFERENCES

Ahmed, S., & Carpenter, P. J. (2003). Geophysical response of filled sinkholes, soil pipes and associated bedrock fractures in thinly mantled karst, east-Central Illinois. *Environmental Geology*, *44*, 705–716. https://doi.org/10.1007/s00254-003-0812-3

Benito, G., Gutiérrez, M., & Sancho, C. (1993). The influence of physicochemical properties on erosion processes in badland areas, Ebro basin, NE-Spain. *Zeitschrift für Geomorphologie*, *37*, 199–214.

Bernatek-Jakiel, A., Bruhans, J., Vojtíšek, J., Stolarczyk, M., & Zaleski, T. (2020). Sediment detachment in piping-prone soils: Cohesion sources and potential weakening mechanisms. *Earth Surface Processes and Landforms*, *45*, 3185–3201. https://doi.org/10.1002/esp.4959

Bernatek-Jakiel, A., Kacprzak, A., & Stolarczyk, M. (2016). Impact of soil characteristics on piping activity in a mountainous area under a temperate climate (Bieszczady Mts., eastern Carpathians). *Catena*, *141*, 117–129. https://doi.org/10.1016/j.catena.2016.03.001

Bernatek-Jakiel, A., & Kondracka, M. (2016). Combining geomorphological mapping and near surface geophysics (GPR and ERT) to study piping systems. *Geomorphology*, *274*, 193–209. https://doi.org/10.1016/j.geomorph.2016.09.018

Bernatek-Jakiel, A., & Kondracka, M. (2019). Detection of soil pipes using ground penetrating radar. *Remote Sensing*, *11*, 1864. https://doi.org/10.3390/rs11161864

Bernatek-Jakiel, A., & Poesen, J. (2018). Subsurface erosion by soil piping: Significance and research needs. *Earth-Science Reviews*, *185*, 1107–1128. https://doi.org/10.1016/j.earscirev.2018.08.006

Botschek, J., Krause, S., Abel, T., & Skowronek, A. (2002). Piping and erodibility of loessic soils in Bergisches land, Nordrhein-Westfalen. *Journal of Plant Nutrition and Soil Science*, *165*, 242–246.

Botschek, J., Maimann, B., & Skowronek, A. (2000). Stofftransporte und relieffformung durch tunnelerosion im Bergischen Land. *Zeitschrift für Geomorphologie*, Suppl.-Bd., *121*, 45–61.

Bovi, R., Moreira, C. A., Rosolen, V. S., Gomes Rosa, F. T., Moreira Furlan, L., & Innocenti Helene, L. P. (2020). Piping process: Genesis and network characterization through a pedological and geophysical approach. *Geoderma*, *361*, 114101. https://doi.org/10.1016/j.geoderma.2019.114101

Cardarelli, E., Cercato, M., De Donno, G., & Di Filippo, G. (2014). Detection and imaging of piping sinkholes by integrated geophysical methods. *Near Surface Geophysics*, *12*, 439–450. https://doi.org/10.3997/1873-0604.2013051

Doolittle, J. A., & Brevik, E. C. (2014). The use of electromagnetic induction techniques in soils studies. *Geoderma*, *223–225*, 33–45. https://doi.org/10.1016/j.geoderma.2014.01.027

Faulkner, H. (2006). Piping hazard on collapsible and dispersive soils in Europe. In J. Boardman & J. Poesen (Eds.), *Soil erosion in Europe* (pp. 537–562). Chichester: John Wiley & Sons, Ltd.. https://doi.org/10.1002/0470859202

Foley, J., Greve, A., Huth, N., & Silburn, M. (2012). Comparison of soil conductivity measured by ERT and EM38 geophysical methods along irrigated paddock transects on black Vertosol soils. In *Proceedings of 16th Agronomy Conference 2012 Capturing Opportunities and Overcoming Obstacles in Australian Agronomy, Armidale, Australia* (pp. 1–4). Gosford, NSW: Australian Society of Agronomy, the Regional Institute.

Giampaolo, V., Capozzoli, L., Grimaldi, S., & Rizzo, E. (2016). Sinkhole risk assessment by ERT: The case study of Sirino Lake (Basilicata, Italy). *Geomorphology*, *253*, 1–9. https://doi.org/10.1016/j.geomorph.2015.09.028

Got, J.-B., André, P., Mertens, L., Bielders, C., & Lambot, S. (2014). Soil piping: Networks characterization using ground-penetrating radar. In *Proceedings of the 15th international conference on ground penetrating radar GPR 2014, June 30–July 4, 2014* (pp. 144–148). IEEE. https://doi.org/10.1109/ICGPR.2014.6970403

Haczewski, G., Kukulak, J., & Bąk, K. (2007). *Budowa geologiczna i rzeźba Bieszczadzkiego Parku Narodowego [Geology and relief of the Bieszczady National Park]*. Wydawnictwo Naukowe Akademii Pedagogicznej w Krakowie.

Heil, K., & Schmidhalter, U. (2015). Comparison of the EM38 and EM38-MK2 electromagnetic induction-based sensors for spatial soil analysis at field scale. *Computers and Electronics in Agriculture*, *110*, 267–280. https://doi.org/10.1016/j.compag.2014.11.014

Holden, J. (2004). Hydrological connectivity of soil pipes determined by ground-penetrating radar tracer detection. *Earth Surface Processes and Landforms*, *29*, 437–442. https://doi.org/10.1002/esp.1039

Holden, J. (2006). Sediment and particulate carbon removal by pipe erosion increase over time in blanket peatlands as a consequence of land drainage. *Journal of Geophysical Research - Earth Surface*, *111*, 1–6. https://doi.org/10.1029/2005JF000386

Holden, J., Burt, T. P., & Vilas, M. (2002). Application of ground-penetrating radar to the identification of subsurface piping in blanket peat. *Earth Surface Processes and Landforms*, *27*, 235–249. https://doi.org/10.1002/esp.316

Joshi, M., Prasobh, P. R., Rajappan, S., Rao, B. P., Gond, A., Misra, A., … Tomson, J. K. (2021). Detection of soil pipes through remote sensing and electrical resistivity method: Insight from southern Western Ghats, India. *Quaternary International*, *575–576*, 51–61. https://doi.org/10.1016/j.quaint.2020.08.021

Kacprzak, A., Szymański, W., & Wójcik-Tabol, P. (2015). The role of flysch sandstones in forming the properties of cover deposits and soils – Examples from the Carpathians. *Zeitschrift für Geomorphologie*, *59*, 227–245. https://doi.org/10.1127/zfg_suppl/2015/S-00182

Kim, D. H., Choi, K. H., Lee, C. H., & Jeong, J. H. (2020). Analysis of small-loop electromagnetic signals to detect subsurface anomaly zones. *Applied Sciences*, *10*, 1–24. https://doi.org/10.3390/APP10186329

Lavoué, F., Van Der Kruk, J., Rings, J., André, F., Moghadas, D., Huisman, J. A., … Vereecken, H. (2010). Electromagnetic induction calibration using apparent electrical conductivity modelling based on electrical resistivity tomography. *Near Surface Geophysics*, *8*, 553–561. https://doi.org/10.3997/1873-0604.2010037

Leslie, I. N., & Heinse, R. (2013). Characterizing soil–pipe networks with pseudo-three-dimensional resistivity tomography on forested hillslopes with restrictive horizons. *Vadose Zone Journal*, *12*, 1–10. https://doi.org/10.2136/vzj2012.0200

Loke, M. H. (2000). *Electrical imaging surveys for environmental and engineering studies*. A practical guide to 2-D and 3-D surveys. Malaysia: Geotomo.

Loke, M. H. (2004). *Tutorial: 2-D and 3-D electrical imaging surveys*. Geotomo Software.

Marey, S., & Tola, E. (2015). Performance of electromagnetic induction meter (EM38-MK2-1) under different working conditions in a Sandy loam soil. *American-Eurasian Journal of Agricultural & Environmental Sciences*, *15*, 1059–1066. https://doi.org/10.5829/idosi.aejaes.2015.15.6.12689

McNeill, J. D. (1980). Electrical conductivity of soils and rocks. In *Technical note TN-5*. Geonics Ltd. http://www.geonics.com/pdfs/technicalnotes/tn5.pdf

Park, D., & Jessop, M. L. (2018). Validation of a new magnetometric survey for mapping 3D subsurface leakage paths. *Geosciences Journal*, *22*, 891–902. https://doi.org/10.1007/s12303-018-0047-7

Patti, G., Grassi, S., Morreale, G., Corrao, M., & Imposa, S. (2021). Geophysical surveys integrated with rainfall data analysis for the study of soil piping phenomena occurred in a densely urbanized area in eastern Sicily. *Natural Hazards*, *108*, 2467–2492. https://doi.org/10.1007/s11069-021-04784-9

Pavoni, M., Sirch, F., & Boaga, J. (2021). Electrical and electromagnetic geophysical prospecting for the monitoring of rock glaciers in the Dolomites, Northeast Italy. *Sensors*, *21*, 1–18. https://doi.org/10.3390/s21041294

Poesen, J. (2018). Soil erosion in the Anthropocene: Research needs. *Earth Surface Processes and Landforms*, *43*, 64–84. https://doi.org/10.1002/esp.4250

Rejiba, F., Schamper, C., Chevalier, A., Deleplancque, B., Hovhannissian, G., Thiesson, J., & Weill, P. (2018). Multiconfiguration electromagnetic induction survey for paleochannel internal structure imaging: A case study in the alluvial plain of the River Seine, France. *Hydrology and Earth System Sciences*, *22*, 159–170. https://doi.org/10.5194/hess-22-159-2018

Samouëlian, A., Cousin, I., Tabbagh, A., Bruand, A., & Richard, G. (2005). Electrical resistivity survey in soil science: A review. *Soil and Tillage Research*, *83*, 173–193. https://doi.org/10.1016/j.still.2004.10.004

Schrott, L., & Sass, O. (2008). Application of field geophysics in geomorphology: Advances and limitations exemplified by case studies. *Geomorphology*, *93*, 55–73. https://doi.org/10.1016/j.geomorph.2006.12.024

Verachtert, E., Maetens, W., Van Den Eeckhaut, M., Poesen, J., & Deckers, J. (2011). Soil loss rates due to piping erosion. *Earth Surface Processes and Landforms*, *36*, 1715–1725. https://doi.org/10.1002/esp.2186

Verachtert, E., Van Den Eeckhaut, M., Martínez-Murillo, J. F., Nadal-Romero, E., Poesen, J., Devoldere, S., … Deckers, J. (2013). Impact of soil characteristics and land use on pipe erosion in a temperate humid climate: Field studies in Belgium. *Geomorphology*, *192*, 1–14. https://doi.org/10.1016/j.geomorph.2013.02.019

Wodajo, L. T., Rad, P. B., Sharif, S. I., Samad, M. A., Mamud, M. L., Hickey, C. J., & Wilson, G. V. (2021). Agrogeophysical methods for identifying soil pipes. *Journal of Applied Geophysics*, *192*, 104383. https://doi.org/10.1016/j.jappgeo.2021.104383

Zajícová, K., & Chuman, T. (2019). Application of ground penetrating radar methods in soil studies: A review. *Geoderma*, *343*, 116–129. https://doi.org/10.1016/j.geoderma.2019.02.024